STRENGTH AND DUCTILITY OF NANOSTRUCTURED SPD METALS

Ruslan Z. VALIEV

Institute of Physics of Advanced Materials,
Ufa State Aviation Technical University,
Ufa, Russia, E-mail: RZValiev@mail.rb.ru

CONTENTS:

Report Documentation Page

Form Approved
OMB No. 0704-0188

1. REPORT DATE	2. REPORT TYPE	3. DATES COVERED
18 MAR 2004	**N/A**	**-**

4. TITLE AND SUBTITLE	5a. CONTRACT NUMBER
Strength And Ductility Of Nanostructured Spd Metals	5b. GRANT NUMBER
	5c. PROGRAM ELEMENT NUMBER
6. AUTHOR(S)	5d. PROJECT NUMBER
	5e. TASK NUMBER
	5f. WORK UNIT NUMBER
7. PERFORMING ORGANIZATION NAME(S) AND ADDRESS(ES) **Institute of Physics of Advanced Materials, Ufa State Aviation Technical University, Ufa, Russia**	8. PERFORMING ORGANIZATION REPORT NUMBER
9. SPONSORING/MONITORING AGENCY NAME(S) AND ADDRESS(ES)	10. SPONSOR/MONITOR'S ACRONYM(S)
	11. SPONSOR/MONITOR'S REPORT NUMBER(S)

12. DISTRIBUTION/AVAILABILITY STATEMENT
Approved for public release, distribution unlimited

13. SUPPLEMENTARY NOTES
See also ADM001672., The original document contains color images.

14. ABSTRACT

15. SUBJECT TERMS

16. SECURITY CLASSIFICATION OF:			17. LIMITATION OF ABSTRACT	18. NUMBER OF PAGES	19a. NAME OF RESPONSIBLE PERSON
a. REPORT	b. ABSTRACT	c. THIS PAGE			
unclassified	**unclassified**	**unclassified**	**UU**	**19**	

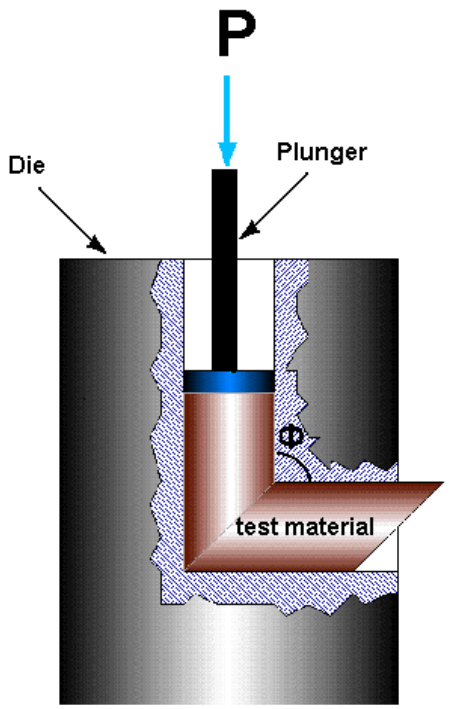

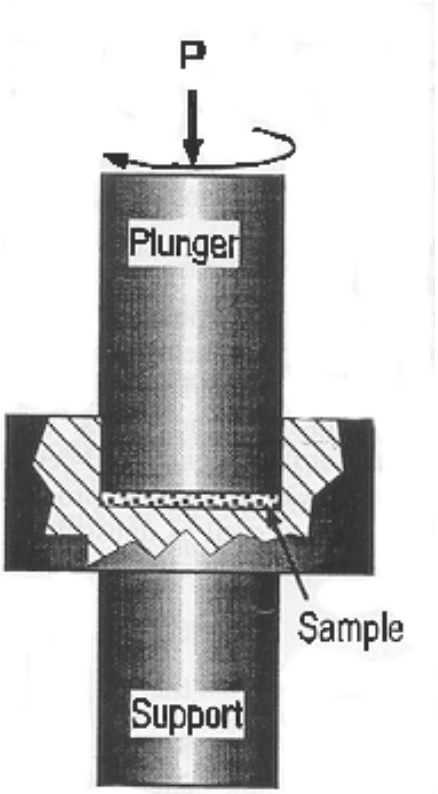

a) Principle of equal-channel angular pressing

b) Principle of torsion straining

Analysis of true strains:

a) Equal-channel angular pressing:

$$\varepsilon = \frac{\mathrm{N} \cdot 2}{\sqrt{3 \cdot \mathrm{ctg}\phi}}$$

N – number of cycles

r– radius of specimen

d – thickness of specimen

b) Torsion straining

$$\varepsilon = \frac{2\pi \cdot n \cdot r}{d}$$

n – number of turns

ECAP PROCESSING

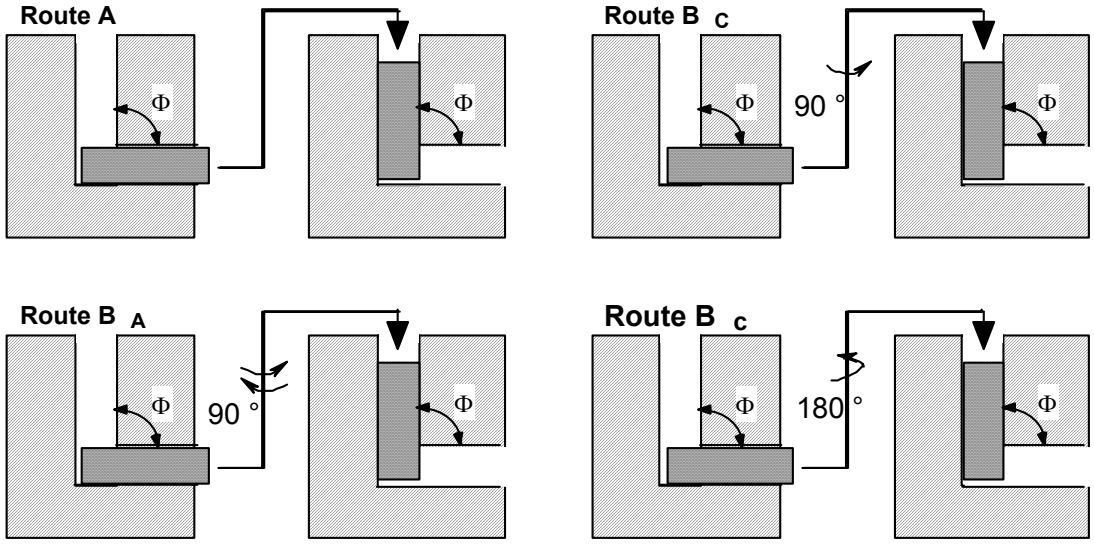

VIEW OF TYPICAL BILLETS PRODUCES BY ECAP (ROUTE Bc)

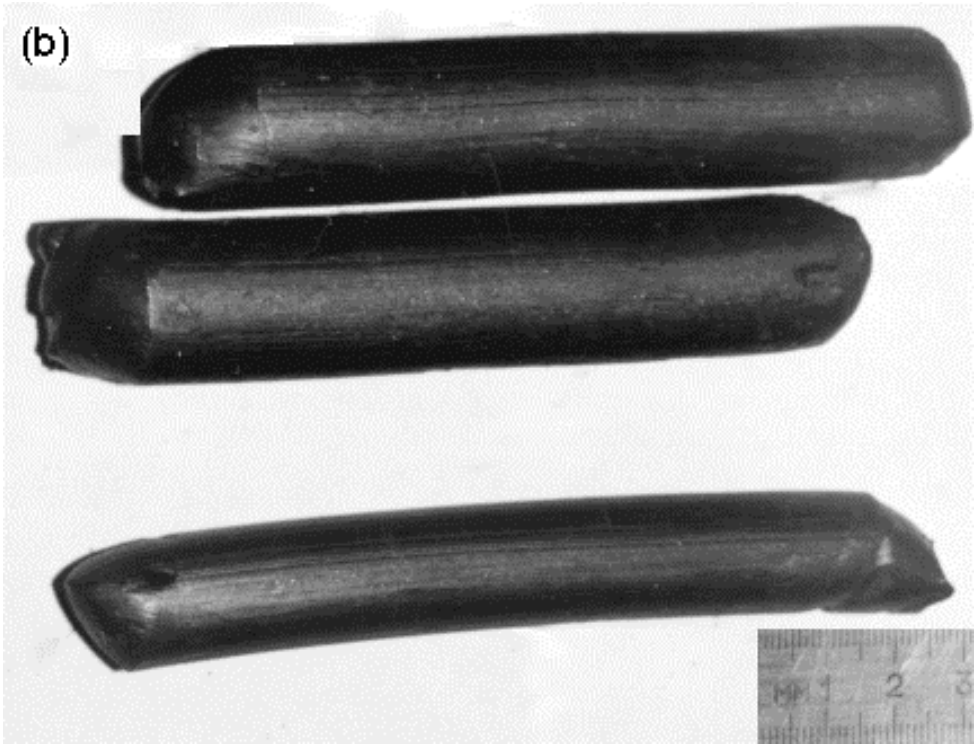

Billets of commercially pure tungsten after ECA pressing in matrix with angle of channels intersection equal to 90^{o}.

Billets out of CP tungsten; (a) before, (b) afer ECA pressing by Route C, 8 passes, using the modification (see the text for details) of SPD processing.

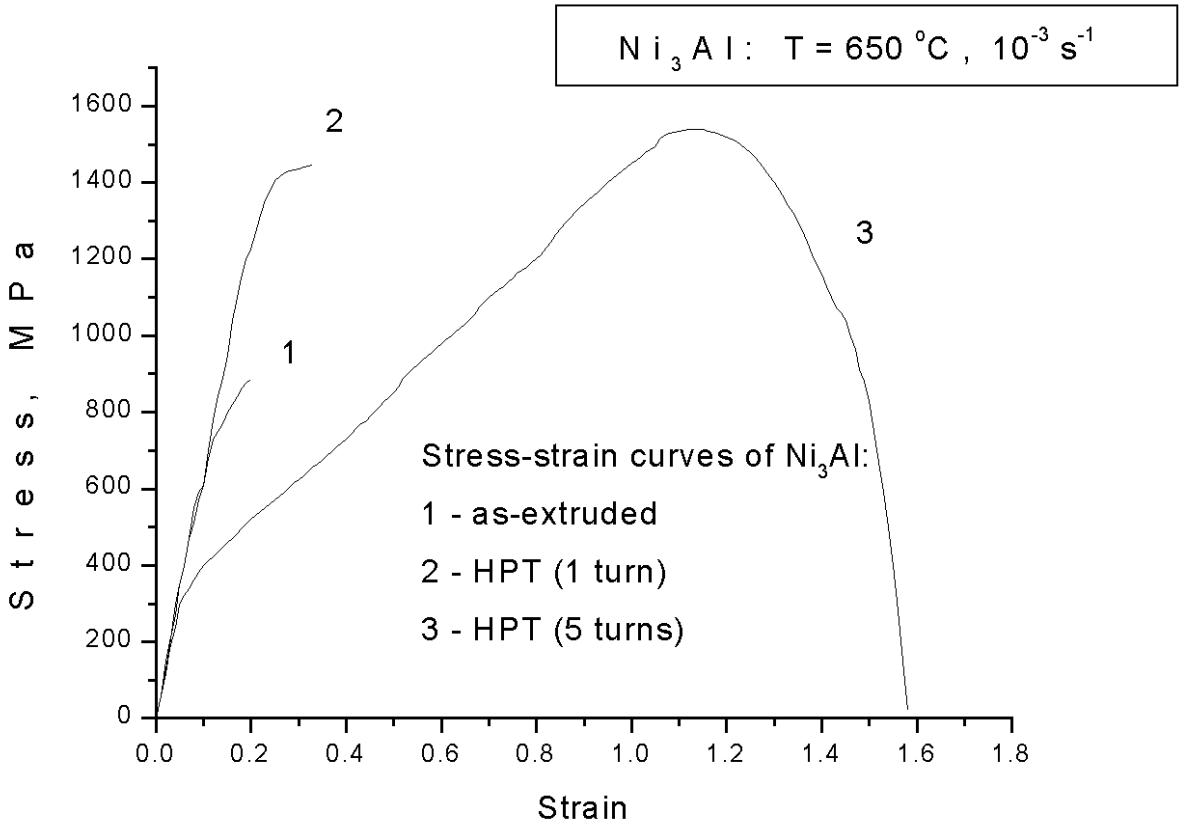
Ni3Al: T = 650 °C, 10-3 s-1
Stress, MPa
Strain
1600
1400
1200
1000
800
600
400
200
0
0.0
0.2
0.4
0.6
0.8
1.0
1.2
1.4
1.6
1.8
1
2
3
Stress-strain curves of Ni3Al:
1 - as-extruded
2 - HPT (1 turn)
3 - HPT (5 turns)

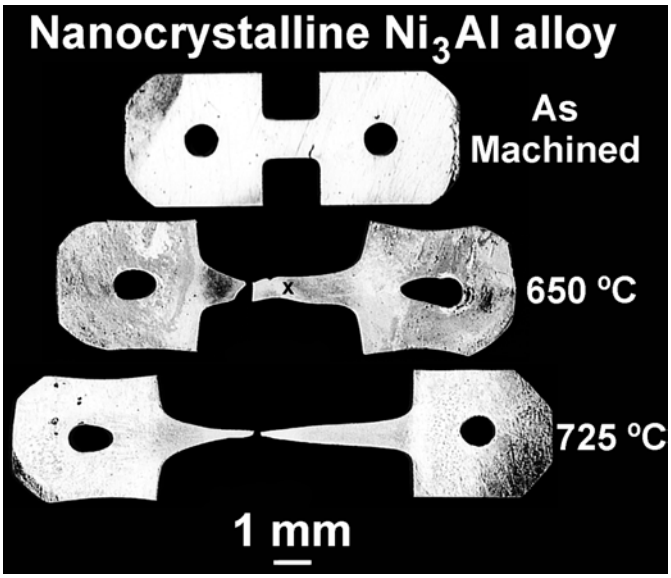

Appearance of the nanocrystalline Ni_3Al before and after tensile tests: as-machined and after pulling at 650°C, $1\times10^{-3}s^{-1}$, 390% elongation (the crossmark on the gauge denotes the region from where the TEM/HREM specimen was prepared) and at 725°C, $1\times10^{-3}s^{-1}$, 560% elongation.

Table Mechanical properties of UFG ECAP metals in comparison with their coarse-grain counterparts.
CG—coarse grain, State 1, 2 and 3 are referred to as "equiaxial", "laminar" and "fragmented" structure attained during ECA-processing, respectively, according to original notations used in the cited papers; N/A— data not available; δ—relative tensile elongation.

	VT1-0	VT1-0[24]				Cu[13,15]			5056 Al–Mg[23,48]	
	UFG 0.3 μm	CG 15 μm	State 1 0.25 μm	State 2 <0.20 μm	State 3 0.15 μm	A 0.2 μm	B 0.2 μm	CG 35 μm	ECAP 0.3 μm	O-temper 25 μm
σ_y, MPa	650	380	625	1020	920	390	440	140	392	122
σ_{UTS}, MPa	810	460	710	1050	1035	410	480	240	442	288
σ_{f0}, MPa	380	238	404	420	460	80	80	65	116	116
σ_{f0}/σ_y	0.58	0.62	0.64	0.41	0.50	0.20	0.18	0.65	0.3	0.95
σ_{f0}/σ_{UTS}	0.48	0.52	0.57	0.40	0.44	0.20	0.17	0.27	0.26	0.58
σ_{f0}/σ_{yCG}	1.00	—	1.06	1.10	1.21	0.57	0.57	—	0.95	—
$\sigma_{f0}/\sigma_{f0CG}$	1.60	−1.70	1.76	1.93	1.23	1.23	—	1.0	—	
δ	0.15	0.26	0.14	0.06	0.10	0.22	0.17	0.46	0.07	0.43
ε_f	0.08	0.09	N/A	N/A	N/A	0.11	0.08	0.27	0.06	0.22
c	−0.54	−0.52	N/A	N/A	N/A	−0.44	−0.49	−0.5	−0.84	−0.84

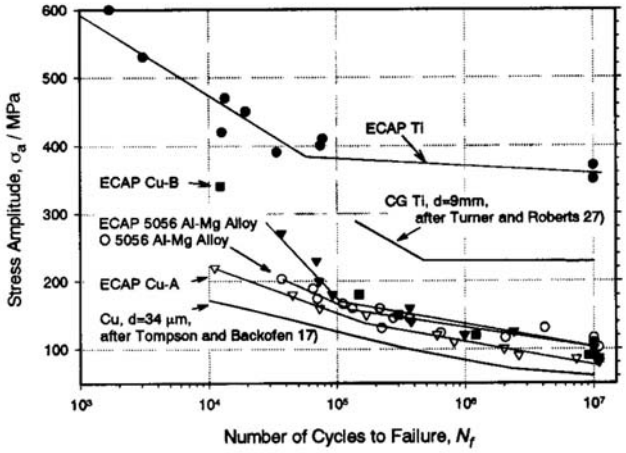

The S–N diagrams of ECAP materials.

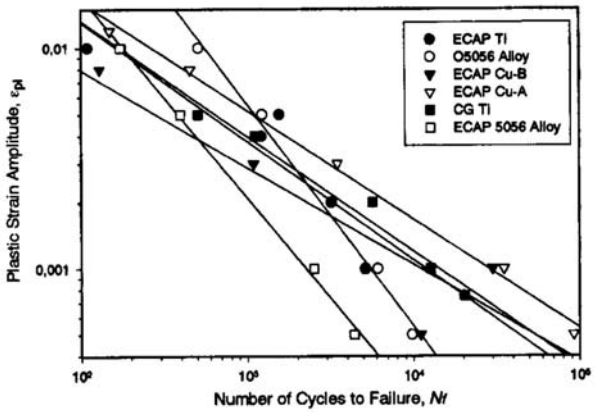

Coffin-Manson plot of Cu, 5056 Al–Mg alloy and Ti before and after ECAP.

Fatigue life

Low-cycle fatigue (LCF) and high-cycle fatigue (HCF) regimes are conventionally distinguished in accord with applied strain amplitudes. In a strain-based approach to fatigue life[37,38] it is naturally to relate the total strain range $\Delta\varepsilon_t$ to the sum of elastic $\Delta\varepsilon_{el}$ and plastic $\Delta\varepsilon_{pl}$ components:

$$\Delta\varepsilon_t = \Delta\varepsilon_{el} + \Delta\varepsilon_{pl} \quad (1)$$

To describe HCF and LCF two following empiric formula link the number of cycles to failure N_f with strain ranges $\Delta\varepsilon_{el}$ and $\Delta\varepsilon_{pl}$ through Basquin (2) and Coffin-Manson (3) law correspondingly:[6,37,38]

$$\frac{\Delta\varepsilon_{pl}}{2} = \frac{\sigma_f}{E}(2N_f)^b \quad (2)$$

$$\frac{\Delta\varepsilon_{pl}}{2} = \varepsilon_f(2N_f)^c \quad (3)$$

where $2N_f$ represents the number of stress reversals, E is the Young's modulus, σ_f and ε_f are the fatigue strength and ductility coefficients and b and c are known as fatigue strength and ductility exponents, respectively. Using the Hook's law the Basquin relation can be rewritten as

$$\frac{\Delta\sigma}{2} = \frac{\Delta\varepsilon_{el}E}{2} = \sigma_f(2N_f)^b \quad (4)$$

and the stress amplitude $\Delta\sigma$ becomes explicitly connected with N_F accounting for the standard Wholer S-N curve (stress vs number cycles to failure). Combining (2) and (3) through (1) one obtains for the total strain amplitude $\Delta\varepsilon_t/2$.

$$\frac{\Delta\varepsilon_t}{2} = \frac{\sigma_f}{E}(2N_f)^b + \varepsilon_f(2N_f)^c \quad (5)$$

Fatigue exponents c and b typically take values $c = -0.5$ to -0.6 and $b = -0.05$ to -0.12.[37,38] ε_F and σ_f correspond often to monotonic fracture strain and stress, respectively, with a fairly good accuracy.

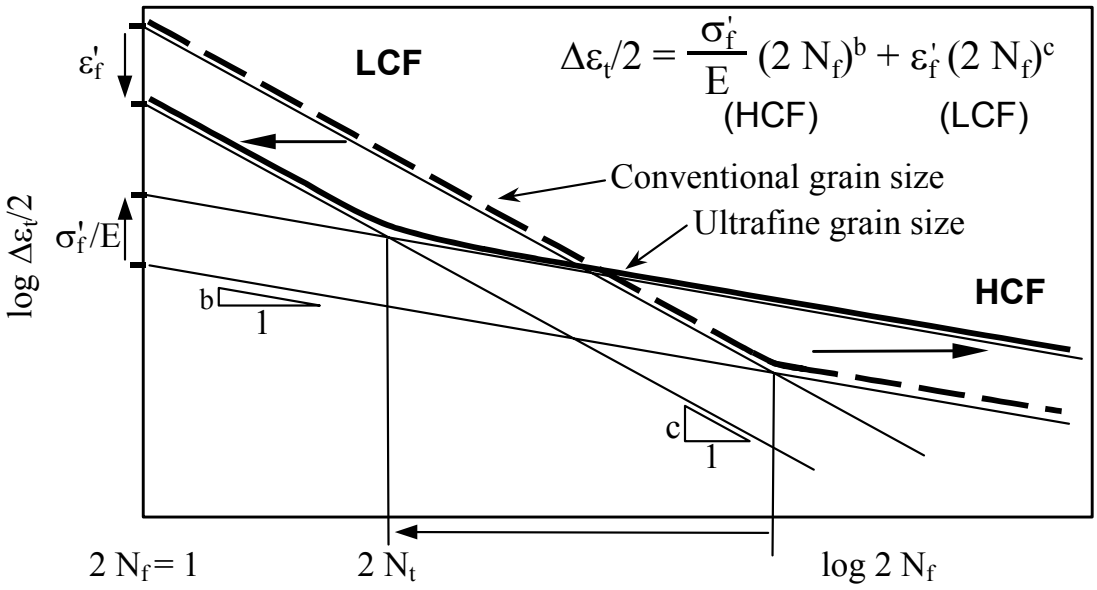

Schematic illustration of enhanced high-cycle fatigue (HCF) life and reduced low-cycle fatigue (LCF) life typical of conventional UFG materials due to increased fatigue strength coefficient σ_f' and reduced fatigue ductility coefficient ε_f', respectively. Note also the reduced transition fatigue life N_t. E: Young's modulus.

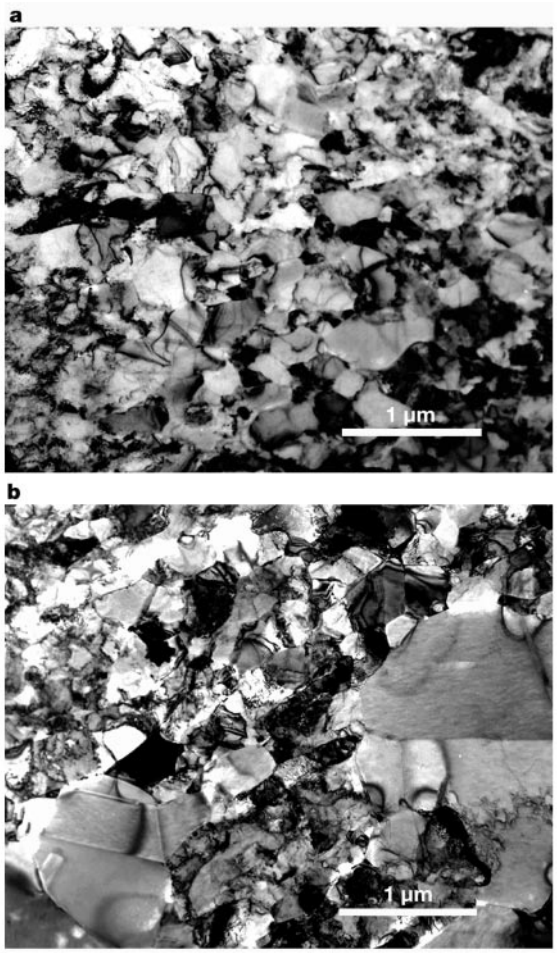

Figure 2 Transmission electron micrographs showing the evolution of the Cu microstructure. Panels a and b show the samples used to obtain the curves D and E in Fig. 1, respectively. After annealing at 180 ºC for 3 min (a), recovery has occurred, and the dislocation density is much reduced. The vast majority of the grains are in the nanocrystalline/ultrafine range, with some recrystallized regions. Heat-treating at 200 ºC for 3 min led to full recrystallization followed by secondary recrystallization (b).

HIGH TENSILE DUCTILITY IN A NANOSTRUCTURED METAL

Yinmin Wang, Mingwei Chen, Fenghua Zhou & En Ma
Johns Hopkins University, USA

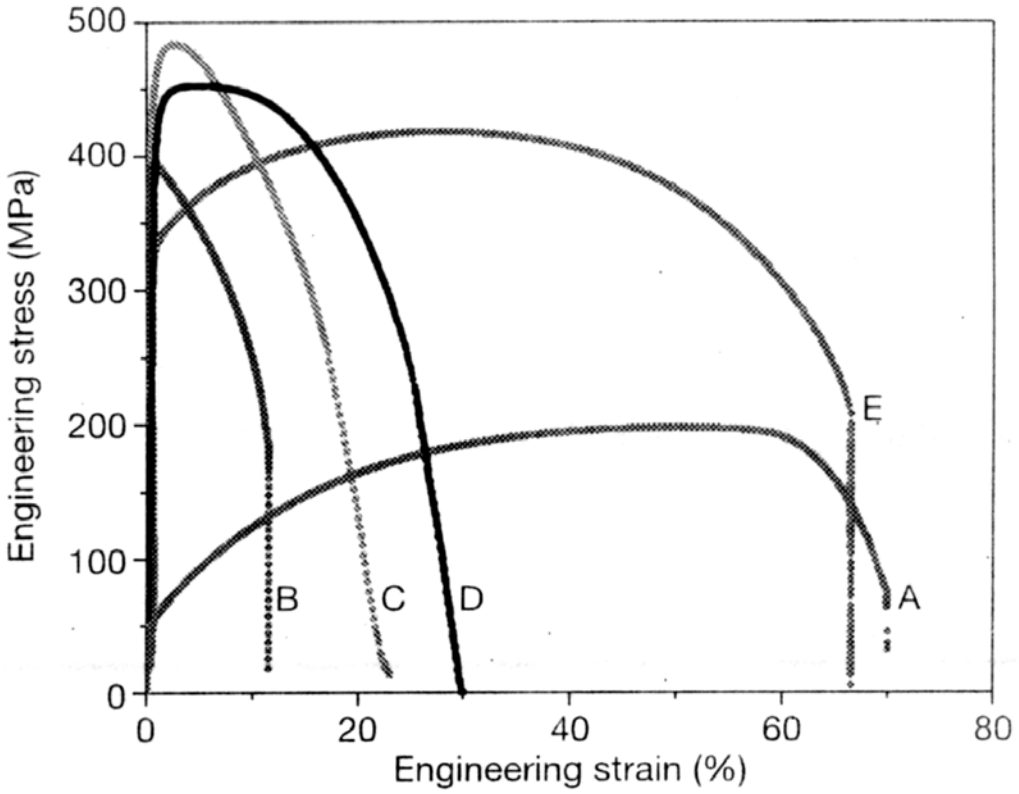

Figure 1 Engineering stress–strain curves for pure Cu. Curve A, annealed, coarse-grained Cu; B, room temperature rolling to 95% cold work (CW); C, liquid-nitrogen-temperature rolling to 93% CW; D, 93% CW + 180 ºC, 3 min.; and E, 93% CW + 200 ºC, 3 min. Note the coexisting high strength and large uniform plastic strain as well as large overall percentage elongation to failure for curve E.

THE MICROSTRUCTURE OF HPT-PRODUCED CP Ti

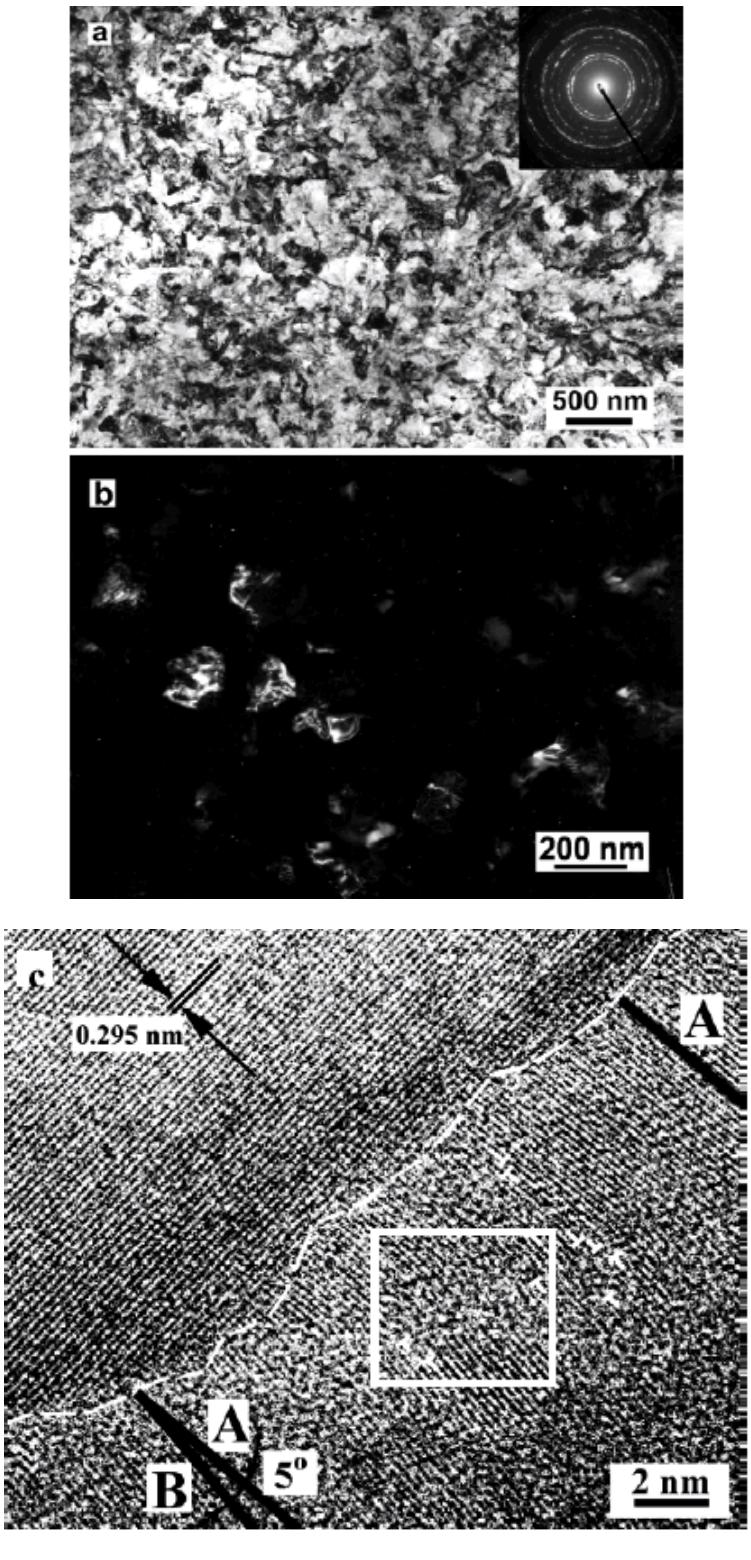

Typical TEM bright field (with SAED as an insert) (a) and dark field (b) micrographs and HREM image (c) of as-processed CP Ti.

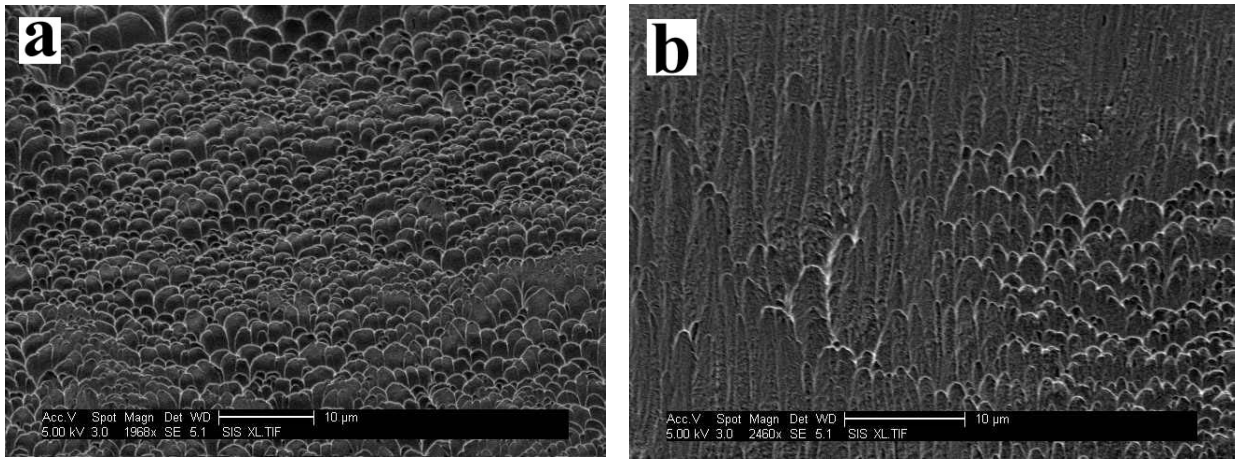

Fracture surfaces of the samples deformed at room temperature: (a) after HPT; (b) after HPT and annealing at 250 ºC for 10 min.

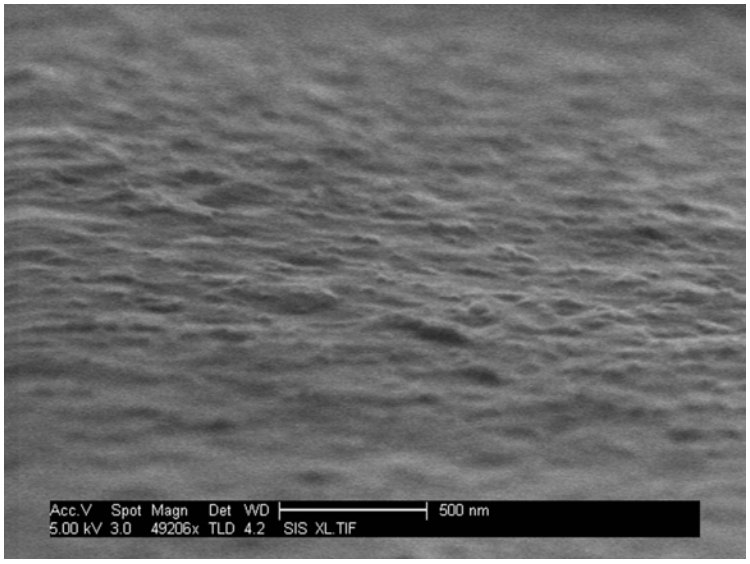

A view of the gage surface after deformation at room temperature.

R.Z. Valiev, A.V. Sergueeva, A.K. Mukherjee, to be published

DEFORMATION TWINNING AND STACKING FAULTS IN NANOSTRUCTURED COPPER

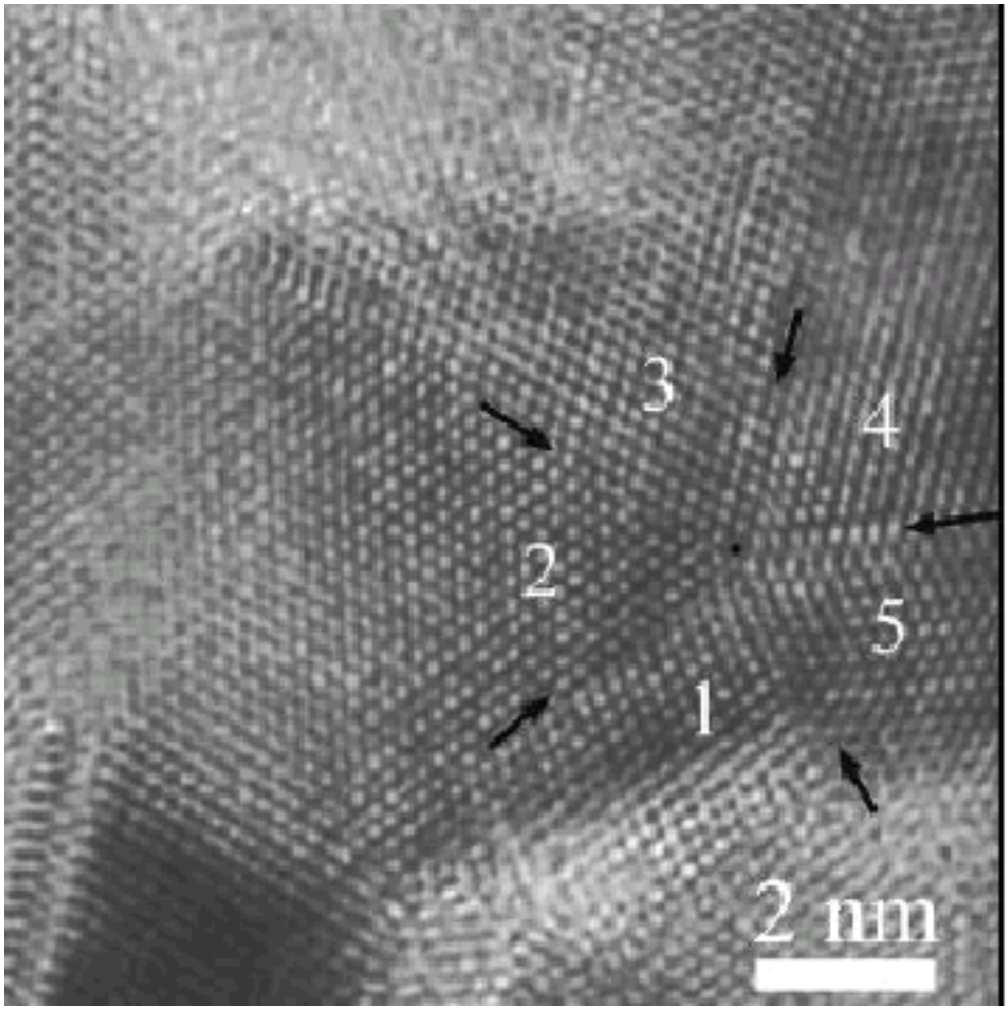

A typical image of a five-fold twin. The twin boundaries are indicated by black arrows and each twin domain is marked with 1 to 5, respectively. The twin center is highlighted with a black full circle.

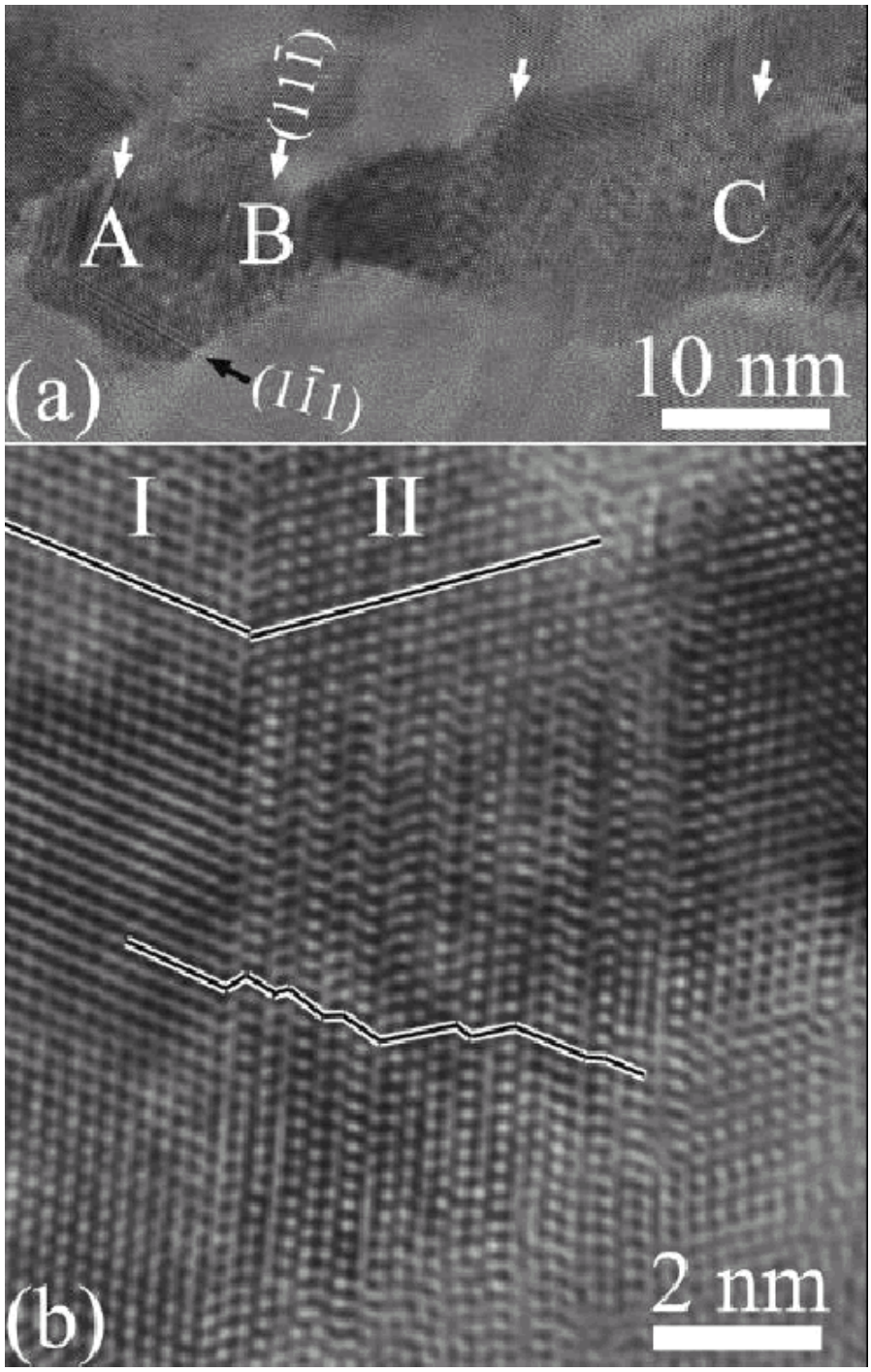

(a) A typical [011] HRTEM image of an elongated crystallite with width varying from smaller than 10 nm to about 20 nm. Twins are seen in this crystallite with most of the twin planes are $(11\bar{1})$ (indicated by white arrows) and one twin plane is $(1\bar{1}1)$ (indicated by a black arrow). Micro-twins and stacking faults are seen in three areas marked A, B, and C, respectively; (b) an enlarged image of area B in (a). The upper part of the image shows only two twin domains I and II, while the lower part of II have a lot of micro-twins and stacking faults with one end of the micro-twins/stacking faults stops within the crystallite.

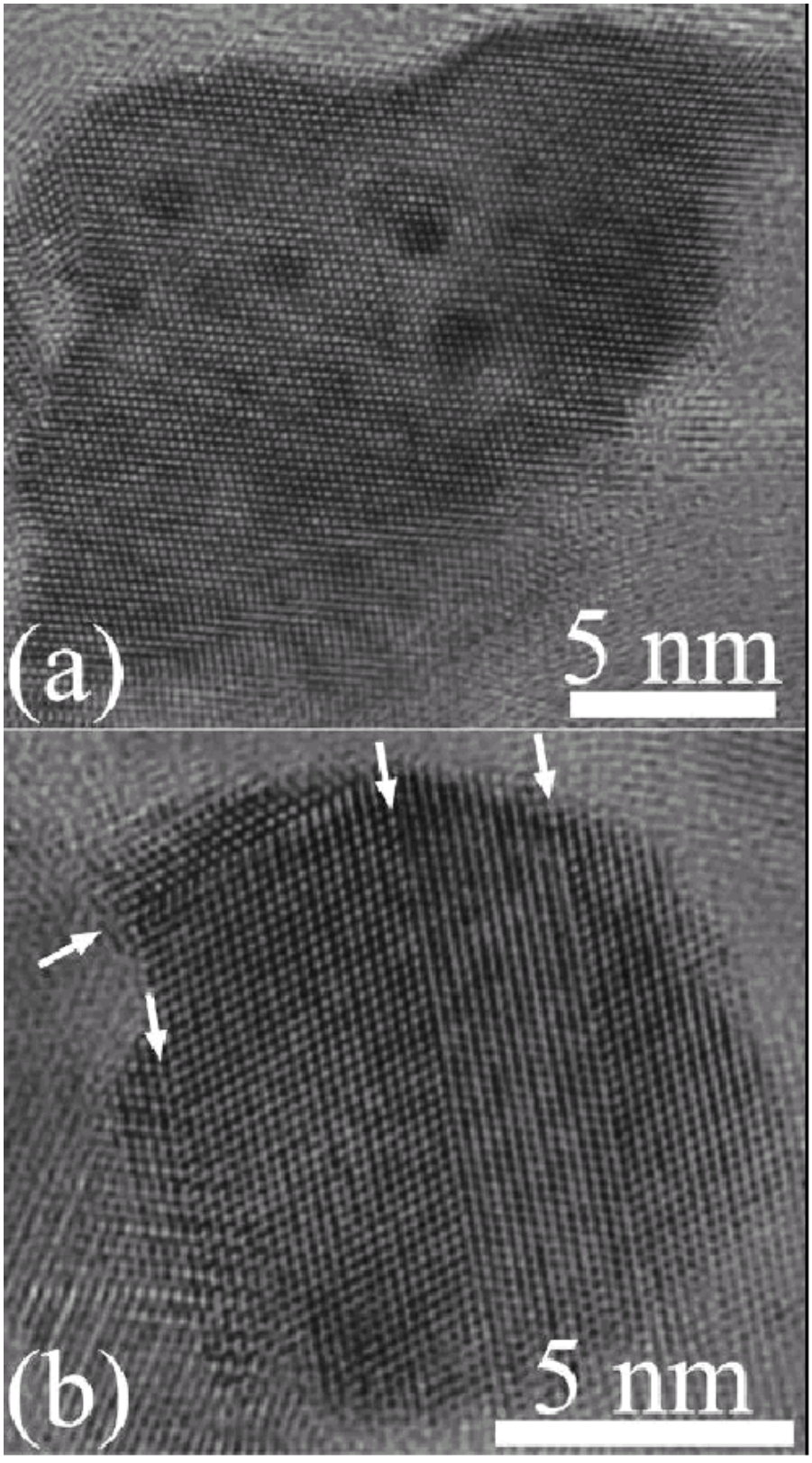

(a) A typical HRTEM image of an equiaxed copper grain without crystalline defect in the grain and (b) a typical HRTEM image of an equiaxed grain with micro-twins. The twin boundaries are indicated by arrows.

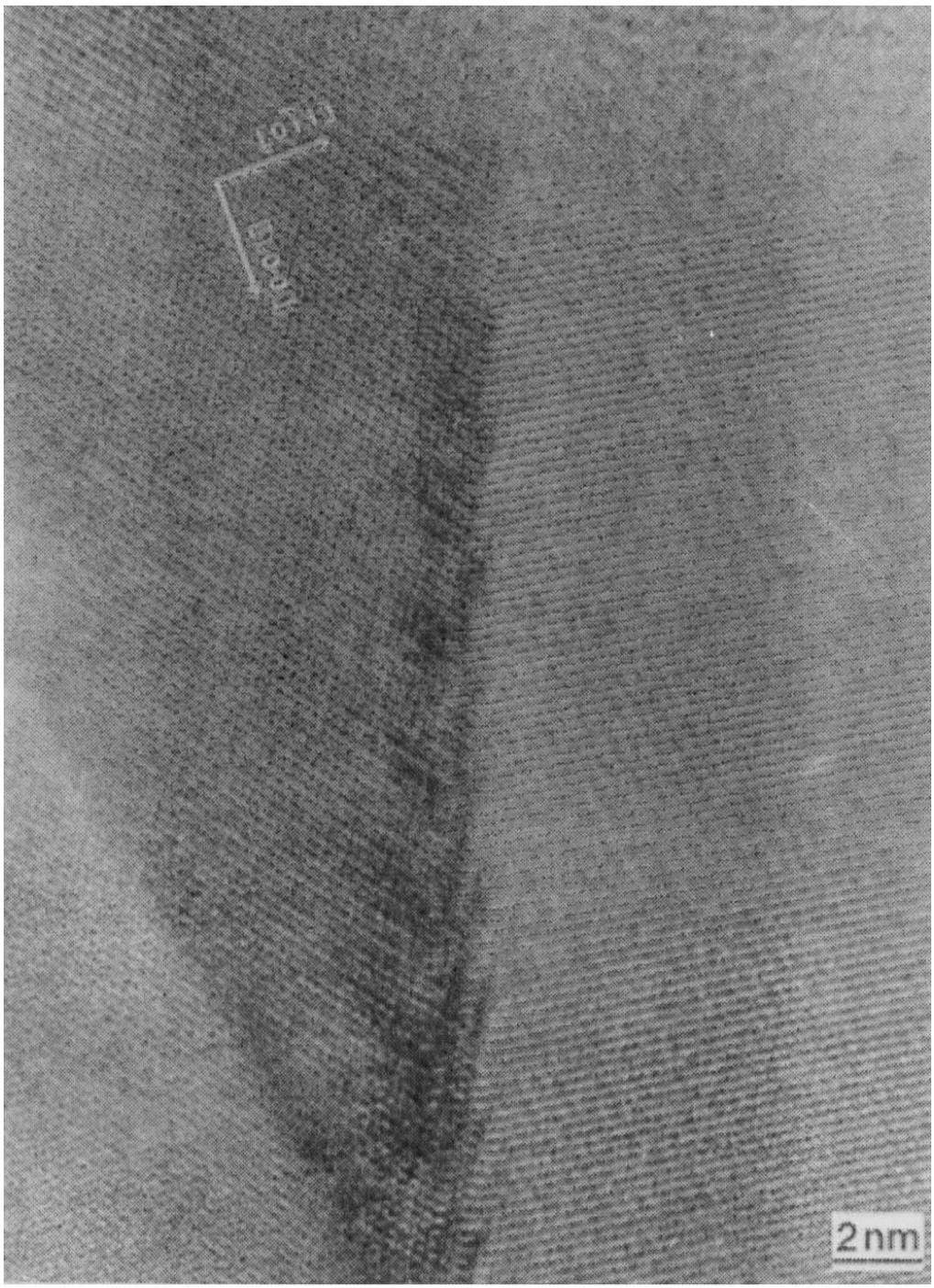

Al-3%Mg, d=100 nm

Z. Horita et al., 1996

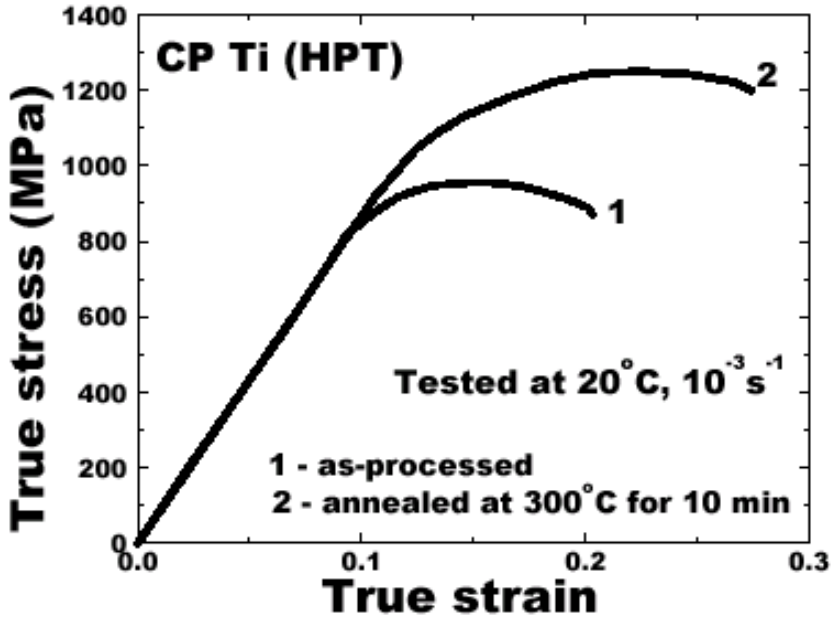

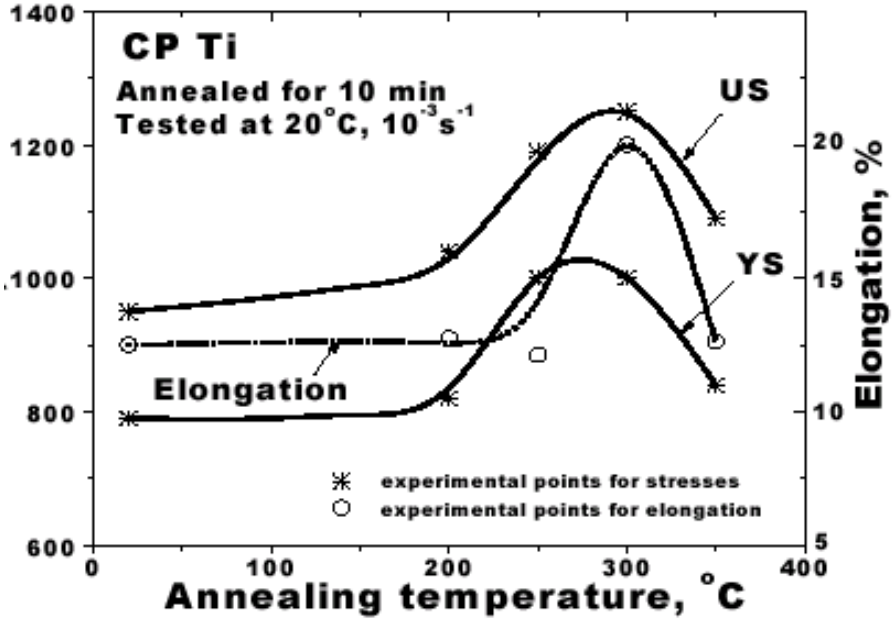

True stress-strain curves of CP Ti after HPT and annealing.

Dependences of ultimate st stress (YS) and elongat annealing temperatu

R.Z. Valiev, A.V. Sergueeva, A.K. Mukherjee, Scripta Mat., in press